

A new search strategy for microquasar candidates using NVSS/2MASS and *XMM-Newton* data

J. A. Combi¹, J.F. Albacete-Colombo^{2,3}, J. Martí¹

¹ Departamento de Física (EPS), Universidad de Jaén, Campus Las Lagunillas s/n, Ed-A3, (23071) Jaén, Spain
e-mail: jcombi@ujaen.es, jmarti@ujaen.es

² Centro Universitario Regional Zona Atlántica (CURZA). Universidad Nacional del COMAHUE, Monseñor Esandi y Ayacucho (8500), Viedma (Rio Negro), Argentina. e-mail: albacete@fcaglp.unlp.edu.ar

³ Osservatorio Astronomico di Palermo, Piazza del Parlamento 1, Palermo (90141), Italy

Received; accepted

ABSTRACT

Aims. Microquasars are ideal natural laboratories for understanding accretion/ejection processes, studying the physics of relativistic jets, and testing gravitational phenomena. Nevertheless, these objects are difficult to find in our Galaxy. The main goal of this work is to increase the number of known systems of this kind, which should allow better testing of high-energy phenomena and more realistic statistical studies of this galactic population to be made.

Methods. We have developed an improved search strategy based on positional cross-identification with very restrictive selection criteria to find new MQs, taking advantage of more sensitive modern X-ray data. To do this, we made combined use of the radio, infrared, and X-ray properties of the sources, using different available catalogs.

Results. We find 86 sources with positional coincidence in the NVSS/XMM catalogs at galactic latitudes $|b| \leq 10^\circ$. Among them, 24 are well-known objects and the remaining 62 sources are unidentified. Out of 86 sources, 31 have one or two possible infrared counterparts in the 2MASS catalog. For the fully coincident sources, whenever possible, we analyzed color-color and hardness ratio diagrams and found that at least 3 of them display high-mass X-ray binary characteristics, making them potential microquasar candidates.

Key words. Radio continuum: general – X-rays: binaries – Infrared: stars – Stars: early-type – Catalogs

1. Introduction

Some of the most attractive objects in the Galaxy are the enigmatic microquasars (MQs). On a smaller scale, they copy the characteristics exhibited by distant quasars (Mirabel & Rodriguez 1999). These systems are X-ray binaries (XRBs) containing compact objects like stellar black holes or neutron stars that accrete matter from a companion star. They are known to emit from radio to X-ray energies (Mirabel & Rodriguez 1994) and possibly up to TeV gamma-ray energies, as in the case of Cygnus X-1 (Albert et al. 2007). Evidence that jets of accreting X-ray binaries can accelerate particles to TeV energies has nevertheless been presented by Corbel et al. (2002). MQs combine two important aspects of relativistic astrophysics: accreting black holes or neutron stars identified by the production of hard X-rays around accreting disks and relativistic radio jets detected by means of their synchrotron emission.

These binary systems are ideal natural laboratories for understanding accretion/ejection process and other gravitational phenomena. However, they seem to be rare objects in our Galaxy. In order to enable more robust statistical studies, it is necessary to increase the number of known MQs. Of the 15 currently confirmed MQs in the galaxy, 6 belong to the high-mass X-ray binary (HMXB) class and 9 are of the low-mass X-ray binary (LMXB) kind (Paredes et al. 2005).

Finding new MQs candidates is not an easy task. Considerable effort in the past has been put in to increasing their number. A few searches for radio-emitting XRB systems and therefore new MQ candidates, based on cross-identifications between radio, infrared, and X-ray catalogs, have been carried out in the past, but without enough success (e.g. Paredes et al. 2002; Ribó et al. 2004). The method of looking for such objects in the Galaxy usually includes a number of steps with very restrictive selection criteria for the sources being investigated. Mainly, a number of competing emission mechanisms and several physical parameters should be associated to the same source or system, and they basically

include the properties of jet emission and XRB behavior. The detection of emission at radio wavelengths could be the signature that such relativistic jets, mainly emitting via incoherent synchrotron emission from very high-energy electrons spiraling in magnetic fields, are present in the object. Ultraviolet and infrared emissions are characteristics displayed by the normal star companions, and X-ray radiation is most efficient at revealing accretion-powered sources, such as binary stars.

As an example, a previous list of MQ candidates obtained from cross-correlation of the radio NVSS catalog (Condon et al. 1998) and the ROSAT Bright Source Catalog (RBSC) sources of the Galactic plane was presented by Paredes et al. (2002). They found 35 possible MQ candidates based on a hardness ratio criterion i.e. $HR1 + \sigma(HR1) \geq 0.9$, where $HR1 = ([0.5 - 2.0 \text{ keV}] - [0.1 - 0.4 \text{ keV}]) / ([0.5 - 2.0 \text{ keV}] + [0.1 - 0.4 \text{ keV}])$. However, since ROSAT soft X-rays are strongly absorbed by the interstellar medium, their resulting list of MQ candidates could be fairly reduced. Given the impossibility that ROSAT will detect X-ray photons at energies above 2.4 keV, and because X-rays in MQs are expected to be highly energetic, such a criterion could not be efficient enough to select possible MQ candidates.

Here, we develop an improved search strategy that is also based on very restrictive, but improved, selection criteria aimed at finding new MQs in the Galaxy. Moreover, we take advantage of modern and more sensitive multiwavelength data. In Sect. 2 we describe the search strategy and sample definition. The general analysis and statistical results are presented in Sect. 3. Finally, we summarize our main conclusions in Sect. 4.

2. Search strategy and sample definition

We performed a positional cross-identification of the NRAO VLA Sky Survey (NVSS¹) catalog (Condon et al. 1998) with the Second *XMM-Newton* Serendipitous Source Catalogue (SXSSC²). The NVSS was observed with the array in D-configuration (DnC configuration for the southernmost fields), which provides an angular resolution of 45". It covers the entire sky from the north pole to declination -40° , and it contains $> 1.8 \times 10^6$ sources (296846 with $|b| \leq 10^\circ$), with a mean source number density of 51.8 per square degree and a source density near the Galactic plane (for $|b| \leq 5^\circ$) of 82.4 per square degree. The rms positional uncertainties in RA and DEC in the NVSS catalog vary from 1" for relatively strong ($S \geq 15$ mJy) point sources to 7" for the faintest ($S \leq 2.3$ mJy) detectable sources. Median positional uncertainties for sources with radio fluxes greater and lower than 15 mJy are, 1".6 and 4".8, respectively. The completeness limit is about 2.5 mJy.

At the X-ray wavelengths, the SXSSC contains 153105 sources for which 24672 sources have $|b| \leq 10^\circ$. In this case the mean source number density, for $|b| \leq 5^\circ$, is 6.85 per square degree. This is a lower value than for NVSS radio sources because the current XMM catalog only covers $\sim 2\%$ of the Galactic plane for $|b| \leq 10^\circ$. The systematic 1 sigma error on the SXSSC detection position ranges between 0".5 and about 1".5. In addition

to the X-ray flux of source, RA and DEC errors essentially depend on the source off-angle with respect to the pointing center of the observation from which it was extracted³. The median flux (in the total photon energy band 0.2 - 12 keV) of the catalog sources is $\sim 2.4 \times 10^{-14} \text{ erg cm}^{-2} \text{ s}^{-1}$; $\sim 20\%$ have fluxes below $1 \times 10^{-14} \text{ erg cm}^{-2} \text{ s}^{-1}$. The use of XMM data is one of the main improvements of this paper over similar, previous works based on ROSAT data (Paredes et al. 2002; Ribó et al. 2004).

Since our intention is to find new galactic MQ candidates in the Galaxy, we adopted a set of selection criteria for NVSS/SXSSC cross-identification summarized as follows:

1. Sources with galactic latitude $\leq 10^\circ$ have been selected from the NVSS and XMM catalogs. This significantly reduces the number of sources to about 16% of the total for both catalogs.
2. No extended radio sources are included in the selection process.
3. We assume that the positional coincidence has high significance when the offset between NVSS/XMM is strictly $R \leq (\epsilon_{\text{XMM}} + \epsilon_{\text{NVSS}})$, where ϵ_{XMM} and ϵ_{NVSS} are the absolute (RA, DEC) error in the position of the XMM and NVSS sources, respectively. For this purpose, we used our IDL (Interactive Data Language⁴) based code to cross-correlate the aforementioned catalogs.
4. After that, we inspected the SIMBAD database and the NASA/IPAC Extragalactic Database (NED) for detecting those previously known sources and well-known MQs in the sample.
5. We further computed the hardness ratio of the whole sample and selected sources with hard X-ray spectra characterized by a power-law model with index $\Gamma \leq 2.5$ typical of LMXB and HMXB systems (e.g. White et al. 1995; Sugizaki et al. 2001).
6. The positions of those NVSS/XMM coincident sources were filtered afterwards with the 2MASS⁵ catalog (Cutri et al. 2003), adopting a cross-identification radius of 4 arcsec, and we used a color-color diagram $(J-H)/(H-K)$ to further constrain our search to likely Galactic objects (see Sec. 3.3 for more details).

3. Main results

After applying the first three criteria, we obtained a total of 86 coincident sources. Figure 1 shows the distribution of the positionally coincident NVSS/XMM sources with Galactic latitudes $|b| \leq 10^\circ$, as a function of the angular separation between the radio and X-ray positions. Positional coincidences of the sources peak at 1".2. Beyond this value, the numerical distribution of positional coincidences falls significantly, producing a decreasing tail towards the largest angular separations. This result is a consequence of the fact that radio sources with the highest fluxes have a well-determined position (around the

³ Details about determining the positional source error can be found at: <http://xmmssc-www.star.le.ac.uk/Catalogue/>

⁴ http://physics.nyu.edu/grierlab/idl_html_help/home.html

⁵ <http://irsa.ipac.caltech.edu/cgi-bin/Gator/>

¹ <http://http://www.cv.nrao.edu/nvss/>

² http://xmm.vilspa.esa.es/external/xmm_data_acc/xsa/index.shtml

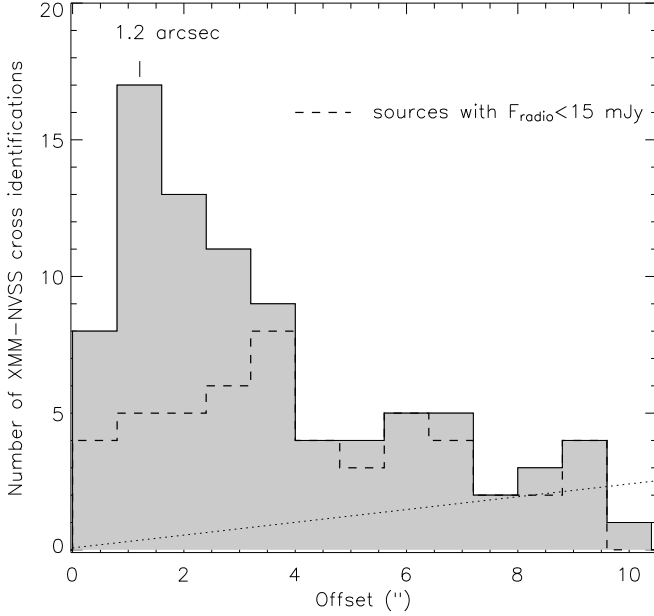


Fig. 1. Numerical distribution of the positionally coincident NVSS/XMM sources as a function of their angular separation. The coincidences were selected adopting an offset between NVSS/XMM positions of $R \leq (\epsilon_{\text{XMM}} + \epsilon_{\text{NVSS}})$, where ϵ_{XMM} and ϵ_{NVSS} are the absolute (RA, DEC) errors in the position of the XMM and NVSS sources, respectively. Of a total 86 sources in the histogram (shaded area), 41 (dashed line) refer to sources with a radio flux lower than 15 mJy. The dotted line refer to the expected XMM-NVSS sources cross-identified by chance.

peak) and that radio sources with the lowest fluxes have large positional uncertainties up to $10''$ and belong to the region with less coincidences. To assess whether the tail is really due to faint NVSS sources, we superimposed a histogram of the angular separation for sources with NVSS flux density below 15 mJy on the numerical distribution. As can be seen, at the largest angular separations, the contribution of weak sources becomes significant.

Finally, we evaluated the number of spurious identifications due to chance alignments N_{chance} , as a function of the identification radius R_{id} . Obviously N_{chance} should be scaled out by sky area A_{search} in the study and by the cross-identification area $A_{\text{id}} = \pi R_{\text{id}}^2$. To compute how N_{chance} increases, we need to increase the identification radius to a larger one: $R_2 = R_{\text{id}} + \Delta R$. Thus A_{id} is increased in an annular region of area $\pi(R_2^2 - R_{\text{id}}^2) = \pi \Delta R (2R_{\text{id}} + \Delta R)$. Assuming (i-) uncorrelated NVSS and XMM-Newton source positions and (ii-) a uniform surface source density of NVSS sources lying in the search area, the total of expected spurious identifications can be written as

$$N_{\text{chance}}(R_{\text{id}}) = \pi N_X \left(\frac{N_{\text{NVSS}}}{A_{\text{search}}} \right) \Delta R (2R_{\text{id}} + \Delta R), \quad (1)$$

where N_X and N_{NVSS} are the total XMM and NVSS sources for Galactic latitude $\leq 10^\circ$. In Fig. 1, ΔR and R_{id} correspond to the bin of the histogram (0.8) and offset (x-axis), respectively. We chose the cut in the identification radius as the largest ($R_{\text{id}} < 10$

arcsec) for which $N_{\text{true}} > N_{\text{chance}}$. As a result, we find that at most 12 coincident sources could be expected by chance in our sample. This value represents about 13% of the matches. In Fig. 1 we overplot a curve with the number of coincidences expected by chance as a function of angular separation.

As a further step, we inspected the SIMBAD and NED database and found that, out of 86 positional coincident sources 24, are well-known objects. These include 10 galaxies (Nakanishi et al. 1997), the cluster of galaxies CIG 0745-19 (Taylor et al. 1994), the globular cluster NGC 6440 (Criscienzo et al. 2006), 3 stars (HD 108, Naze et al. 2004; V*V684 Mon, Rouser et al. 1988; ζ Puppis, Blomme et al. 2003), 3 star forming regions (Gondoin 2006), 2 pulsars (PSR J0737-3039, Chatterjee et al. 2005; PSR J1833-1034, Camilo et al. 2006), the HII region G10.62-0.38 (Hofner & Churchwell 1996), and the remaining 62 objects are unidentified. Out of 15 well-known MQs, 5 have been detected in the NVSS survey, 3 belong to the southern sky and therefore lie outside the survey limit, and the remaining 7 were not detected. None of these 5 radio detections is covered by the XMM-Newton catalog, which is why we did not recover them in this work.

3.1. X-ray colors of NVSS/XMM objects

Statistical studies of high-energy sources based on X-ray colors can be used to classify objects with different spectral-energy distributions belonging to different galactic populations. Thanks to the wider (0.2-12 keV) energy range of the SXSSC, we are able to compute X-ray colors of sources in three different broad-bands, thus helping us better unmask signs of highly energetic processes in our list of positionally coincident NVSS/XMM sources. The resulting properties of the newly-found MQ candidates are presented in the table and plots discussed below.

We use three bands here defined in the catalog: Soft (S: 0.2-1.0 keV), Medium (M: 1.0-2.0 keV), and Hard (H: 2-12.0 keV). Figure 2 shows the count ratio of X-ray colors $H_x = (M-S)/(S+M)$ and $H_y = (H-M)/(H+M)$. While it is difficult to classify individual sources with confidence on the basis of X-ray color alone, we computed and plot the predicted loci for absorbed power-law models with a Γ index ranging from 0 to 4 and an interstellar absorption N_H from 10^{21} to $4 \times 10^{22} \text{ cm}^{-2}$. The grid was calculated with the *Portable Interactive Multi-Mission Simulator* (PIMMS⁶) by using a power-law emission model.

From a direct comparison of the source position with respect to the Γ - N_H grid, we obtained an estimation for the N_H and Γ values, which is a good approximation of the X-ray energy distribution of the sources. Table 1 shows the X-ray properties of the coincident NVSS-XMM sources. The present knowledge of each one is labeled according to the flag-Id numbers in the last column of the table. Figure 2 shows the ratios of source counts in different spectral bands. In this image three microquasars (LS 5039, GRO 1655-40, and GX339-4) that are undetected in the NVSS survey or not strictly coincident with their SXSSC counterparts are indicated for comparison pur-

⁶ <http://heasarc.gsfc.nasa.gov/docs/software/tools/pimms.html>

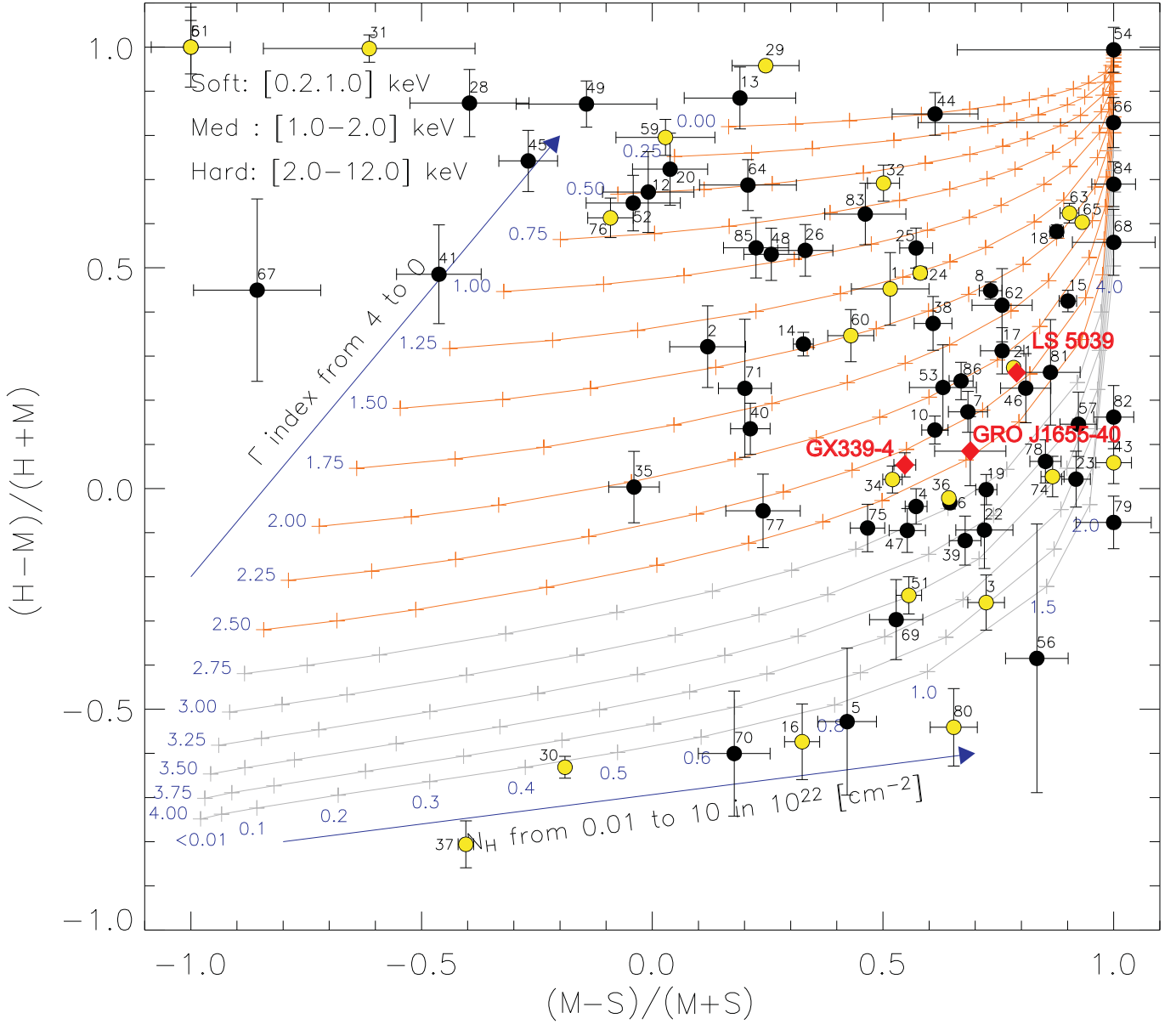


Fig. 2. Ratios of source counts in different spectral bands. Soft (S_x : 0.5-2.0 keV), Medium (M_x : 2.0-4.5 keV), and Hard (H_x : 4.5-12.0 keV). $(S - M)/(S + M)$ on X-axis and $(H - M)/(H + M)$ on Y-axis. The 1σ error bars are shown for all the sources. Filled (black) points correspond to unidentified objects in our sample while those shown as open (yellow) points correspond to already known sources. Well-known microquasars are also indicated as (red) diamonds.

poses. The position of the three MQs in the figure agree very well with the values of Γ and N_H obtained by several authors using *XMM-Newton* data; e.g., Bosch-Ramon et al. (2007) in LS 5039; Miller et al. (2004) for GX339-4; and Diaz Trigo et al. (2007) for GRO J1655-40. For sources 9, 11, 27, 28, 29, 31, 33, 37, 42, 45, 49, 50, 54, 55, 56, 58, 61, 72, 73, 79, 80, 82, and 84 that lie outside the N_H - Γ grid, the power-law model does not provide an adequate fit.

In order to distinguish different types of objects and to check the reliability of our analysis, we compared the values of N_H and Γ of the sources with the classification scheme presented by Prestwich et al. (2003). For this purpose, we applied the hardness ratio classification using the band definition by Prestwich et al. (2003) exactly. We computed $HR_{\text{soft}} =$

$(M_x - S_x)/T_x$ and $HR_{\text{hard}} = (H - M)/T$, where S_x : 0.3-1., M_x : 1-2, H_x : 2-8 keV, and T_x are the total counts in all three bands combined.

We find that sources with $\Gamma < 1$ and $1 < \Gamma < 2.5$, with a small dependence on the N_H , lie in the HMXB and LMXB loci, respectively. This interpretation agrees with being HMXBs known to display spectra in the 1-10 keV region, well-represented by a power-law index Γ of 1-2 (White et al. 1995), and also often with a high variable intrinsic absorption to reach Γ values as low as ~ 0.3 . We have 39 NVSS-XMM sources in this regime, with only 10 of them well-known objects (1, 21, 24, 32, 34, 59, 60, 63, 65 and 76). The remaining 29 objects (2, 7, 8, 10, 12, 13, 14, 15, 17, 18, 20, 25, 26, 35, 38, 40, 44, 46, 48, 52, 53, 62, 64, 71, 77, 81, 83, 85, 86) could be low-mass

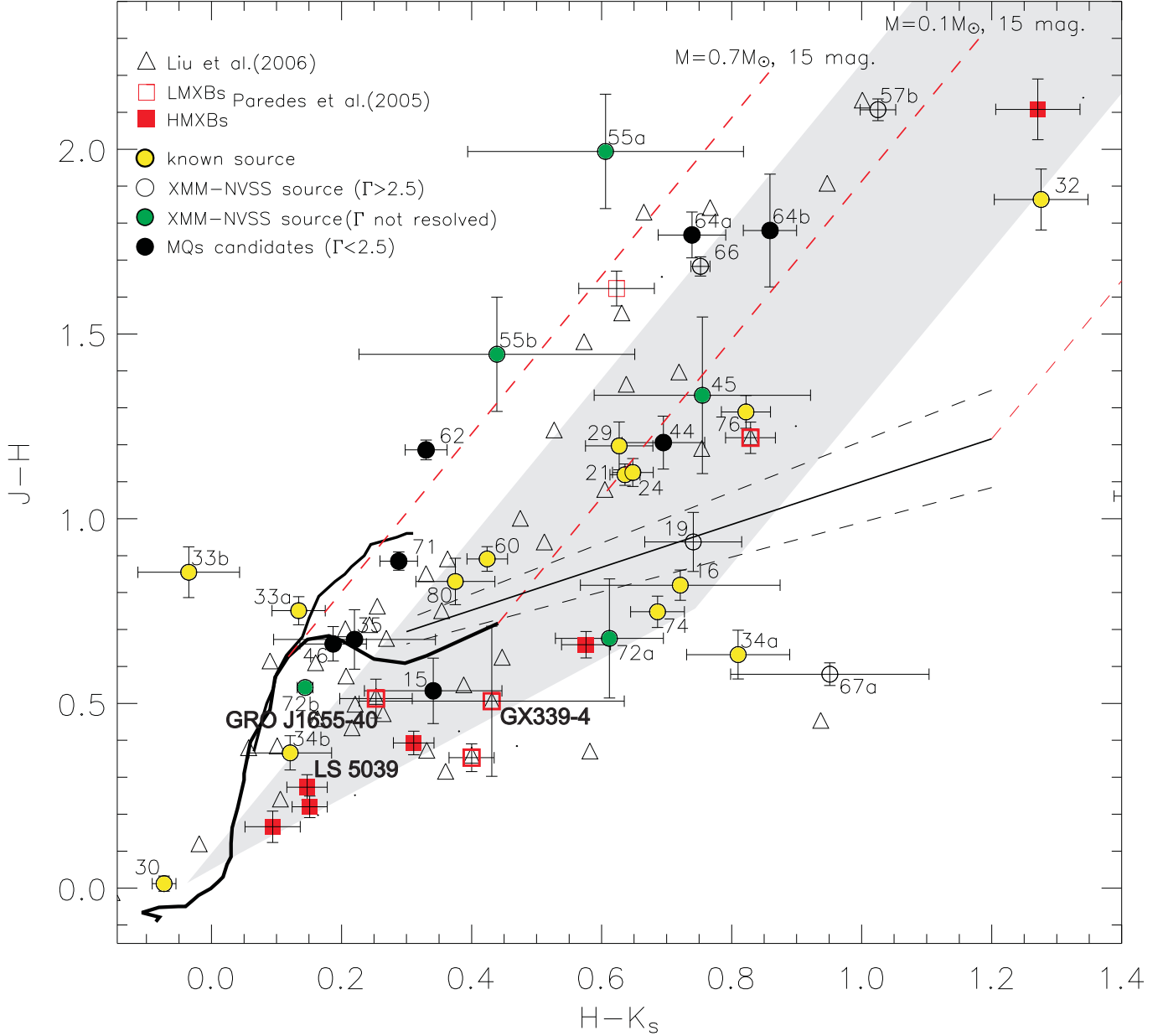


Fig. 3. Color-color diagram ($J - H/H - K$) of the positional correlated sources. The intrinsic colors of the main sequence (Siess et al. 2000), the CTTS locus (Meyer et al. 1997), and giant stars are shown, as well as the slope and magnitude of the interstellar reddening vector ($A_V=15$ mag). Well-known MQs (in red) and HMXB systems (white open squares) are also shown. The most promising MQ candidates (indicated as black points) lie inside the region shaded in grey.

or high-mass XRB systems. As expected, LS 5039, GX339-4, and GRO J1655-40 lie within this zone.

3.2. Cross-identification of NVSS/XMM with the 2MASS near-IR data

Since it is incomplete to define MQ candidates based on the individual X-ray colors alone, a more accurate perspective on the near-IR properties of the 86 NVSS-XMM objects can help us improve our knowledge about the nature of the sources, as well as to concentrate efforts on those objects with more reliable MQ characteristics.

Given that 2MASS photometry is only complete to K_s band ≈ 14.8 mag, the cross-correlation between our NVSS-XMM source list with the 2MASS database is very restrictive. However, the availability of near-IR observations of the whole sky provides an excellent opportunity to focus on our MQ candidate sample. The cross-identification of the 86 NVSS/XMM sources with the 2MASS catalog was performed using a search radius $R \sim 4''$ (the 90% uncertainty radius in the X-ray position). In addition, one additional restrictive criteria was applied. Accretion disks with different ranges of accretion rates

and viewing angles account for intrinsic near-infrared excesses distributed in a narrow range in the $(J-H)$ vs $(H-K_s)$ diagram (Meyer et al. 1997). We also use this information to constraint the location of MQ candidates based on their near-IR properties.

The resulting sample now contains 31 sources with one or two 2MASS counterpart candidates. Of these, 16 are already cataloged sources (see flag-Id in Table 1), while the remaining 15 objects appear as unidentified. The fact that some of the candidates show no IR counterpart in the 2MASS catalog does not mean that no IR counterpart exists. They could simply be highly obscured objects. Hereafter, we only focus our attention on these coincident NVSS-XMM sources with 2MASS counterparts. A deeper search for IR counterparts for the rest of the sources undetected in the 2MASS counterpart is in progress.

3.3. Near infrared color-color analysis

From the near-IR photometric measurements, we can locate objects in the $(J-H)$ vs $(H-K_s)$ color-color diagram. This allows us to distinguish objects with small, intermediate, or large near-infrared excess, as well as those with intrinsic K_s excess that are probably produced by the presence of a disk-star structure (Meyer et al. 1997).

Figure 3 shows the color-color diagram $(J-H)-(H-K_s)$ for the sources. To facilitate the identification in the diagram, we used for each source the number assigned in Table 1 and Figure 2. We also plot the near-IR colors of known HMXB systems (Liu et al. 2006), well-known MQs (Paredes et al. 2005), the classical T-Tauri stars (CTTS) locus of Meyer et al. (1997), and two reddening vectors with lengths corresponding to $A_V=15$ mag. It is interesting to note that, while MQs in HMXB systems have an approximate lineal behavior in the diagram, LMXBs have a more random distribution.

This suggests that the most promising MQ candidates in HMXB systems could follow the HMXB loci, which might be placed following the direction of reddening vectors because of the different values of the interstellar absorption. We indicate this region of possible MQ candidates with a grey region in Fig 3. Six sources (36, 49, 50, 51, 57, and 59) with infrared counterparts fall outside the limits of the diagram. Of these, 4 are well-known objects (see flag-Id in Table 1) and 2 of them do not fulfill the characteristics required to be low-mass or high-mass X-ray systems; therefore, they were discarded from our analysis. As can be seen, only three sources (15, 44, and 64b) lie within the suggested MQ grey region.

Finally, it is worth noting that, in the hardness ratio classification by (Prestwich et al. 2003), the sources 15, 44, and 64 show values of HR_{soft} 0.27, 0.06, and 0.05 and HR_{hard} 0.42, 0.83, and 0.60, respectively. Therefore, these sources lie in the loci of HMXBs.

4. Summary

In this work we have presented an improved search strategy for finding new MQ candidates based on positional cross-identifications. By analyzing radio and modern more sensitive X-ray data, we found 86 positional-coincidence sources in the

NVSS and XMM catalog, with galactic latitudes $|b| \leq 10^\circ$. Among them, 24 are well-known objects and the rest of the 62 sources are unidentified. Out of the 86 sources 31 have one or two infrared counterpart candidates in the 2MASS catalog. For all the sources, when possible, the hardness ratio was used to assess the low-mass or high-mass XRB properties of the objects. At least 29 unidentified objects fulfill these characteristics. Using the 2MASS counterpart of well-known MQs, we found that MQs with a high-mass nature follow a lineal behavior in the infrared color-color diagram, while LMXB MQs display a more random distribution. Based on this information, we suggest a possible region in the infrared diagram for new MQ candidates. As a result, we found 3 objects that we propose as likely galactic HMXBs and MQ candidates. A follow-up study of these three sources will be reported on a future paper (Combi et al. 2007).

Finally, it is important to mention that the whole analysis carried out here only covers a minute fraction of the expected MQ candidates. The NVSS survey does not cover all of the sky. It is complete up to -40° in declination. In addition, the current XMM catalog only represents $\sim 2\%$ of the galactic plane ($|b| \leq 10^\circ$). Thus, a naive extrapolation of the 3 MQ candidates to the whole Galactic plane suggests that about 120 new candidates could be expected in the future.

Acknowledgements. We thank the anonymous referee for her/his insightful comments and constructive suggestions that lead to a substantial improvement of the manuscript. We also thank Valenti Bosch-Ramón and Marc Ribó for useful discussions, and the staff of the Osservatorio Astronomico di Palermo where part of this research was carried out. J.A.C. is a researcher of the programe *Ramón y Cajal* funded jointly by the Spanish Ministerio de Educación y Ciencia (former Ministerio de Ciencia y Tecnología) and Universidad de Jaén. J.F.A.C. is a researcher of the Consejo Nacional de Investigaciones Científicas y Tecnológicas (CONICET), Argentina. The authors acknowledge support by the DGI of the Spanish Ministerio de Educación y Ciencia under grants AYA2004-07171-C02-02, FEDER funds and Plan Andaluz de Investigación of Junta de Andalucía as research group FQM-322.

References

- Albert, J., et al. 2007, *ApJ*, 665, L51
- Blomme, R., van de Steene, G. C., Prinja, R. K., Runacres, M. C., & Clark, J. S. 2003, *A&A*, 408, 715
- Bosch-Ramon, V., Motch, C., Ribo, M., Lopes de Oliveira, et al., *astro-ph/0703499*.
- Camilo, F., Ransom, S. M., Gaensler, B. M., et al. 2006, *ApJ*, 637, 456
- Chatterjee, S., Goss, W. M., & Briskin, W. F. 2005, *ApJ*, 634, L101
- Combi, J.A., Albacete Colombo, J.F., et al. 2007, in preparation.
- Condon, J. J., Cotton, W. D., Greisen, E. W., Yin, Q. F., Perley, R. A., Taylor, G. B., & Broderick, J. J. 1998, *AJ*, 115, 1693
- Corbel, S., Fender, R. P., Tzioumis, A. K., et al. 2002, *Science*, 298, 196
- Criscienzo, M. D., Caputo, F., Marconi, M., & Musella, I. 2006, *VizieR Online Data Catalog*, 736, 51357

- Cutri, R. M., et al. 2003, The IRSA 2MASS All-Sky Point Source Catalog, NASA/IPAC Infrared Science Archive. <http://irsa.ipac.caltech.edu/applications/Gator/>,
Díaz Trigo, M., Parmar, A. N., et al., 2007, A&A, 462, 657
Dubus, G. 2006, A&A, 456, 801
Gondoin, P. 2006, A&A, 454, 595
Hofner, P., & Churchwell, E. 1996, VizieR Online Data Catalog, 412, 283
Liu, Q. Z., van Paradijs, J., & van den Heuvel, E. P. J. 2006, VizieR Online Data Catalog, 345, 51165
Meyer, R. M., Calvet, N., & Hillenbrand, L. A., 1997, ApJ, 114, 288.
Miller, J. M., et al. 2004, ApJ, 606, L131
Mirabel, I. F., & Rodríguez, L. F. 1994, Nature, 371, 46
Mirabel, I. F., & Rodríguez, L. F. 1999, ARA&A, 37, 409
Nakanishi, K., Takata, T., Yamada, T., Takeuchi, T. T., Shiroya, R., Miyazawa, M., Watanabe, S., & Saito, M. 1997, ApJS, 112, 245
Nazé, Y., Rauw, G., Vreux, J.-M., & De Becker, M. 2004, A&A, 417, 667
Paredes, J. M., Ribó, M., & Martí, J. 2002, A&A, 394, 193
Paredes, J. M. 2005, Chinese Journal of Astronomy and Astrophysics, 5, 121
Prestwich, A. H., Irwin, J. A., Kilgard, R. E., et al., 2003, ApJ, 595, 719
Ribó, M., Paredes, J. M., Martí, J., Casares, J., Bloom, J. S., Falco, E. E., Ros, E., & Massi, M. 2004, Revista Mexicana de Astronomía y Astrofísica Conference Series, 20, 23
Roeser, S., & Bastian, U. 1988, A&AS, 74, 449
Siess, L., Dufour, E., & Forestini, M. 2000, A&A, 358, 593
Skrutskie, M. F., et al. 2006, AJ, 131, 1163
Sugizaki, M., Mitsuda, K., Kaneda, H., Matsuzaki, K., Yamauchi, S., & Koyama, K. 2001, ApJS, 134, 77
Taylor, G. B., Barton, E. J., & Ge, J. 1994, AJ, 107, 1942
White, N.E., Nagase, F., & Parmar, A. N. 1995, in X-ray Binaries ed. W.G.H. Lewin, Cambridge Univ. Press, 1

Table 1: X-ray properties of NVSS/XMM-Newton cross-correlated sources

Src #	IAU name 2XMMp J+	Coordinates J2000		Hardness ratio		X-ray properties			flag Id.
		RA	DEC	HR _x	HR _y	N _H [10 ²²]	Γ	Flux[10 ⁻¹⁴]	
1	000647.1+633603	00:06:47.17	63:36: 3.30	0.52	0.45	0.38	1.30	0.45 ± 0.3	2
2	001914.6+592006	00:19:14.61	59:20: 6.26	0.12	0.32	0.18	1.36	0.68 ± 0.4	1
3	002108.8+591132	00:21: 8.89	59:11:32.31	0.72	-0.26	1.20	3.70	1.27 ± 0.5	3
4	011050.6+601203	01:10:50.59	60:12: 4.01	0.57	-0.04	0.70	2.68	3.01 ± 0.7	1
5	014032.1+581137	01:40:32.18	58:11:37.21	0.42	-0.53	0.82	4.20	2.03 ± 2.1	1
6	021808.0+570502	02:18: 8.08	57:05: 2.40	0.65	-0.03	0.79	2.72	14.20 ± 1.0	1*
7	021916.6+570200	02:19:16.64	57:02: 0.28	0.68	0.17	0.77	2.20	1.38 ± 0.4	1*
8	021939.0+622721	02:19:39.02	62:27:21.41	0.73	0.45	0.70	1.68	16.06 ± 1.5	1
9	022054.3+565720	02:20:54.38	56:57:20.03	—	—	—	—	2.74 ± 2.3	1
10	022147.6+571119	02:21:47.69	57:11:19.53	0.61	0.13	0.68	2.20	3.73 ± 0.6	1
11	023656.7+615759	02:36:56.77	61:57:59.72	—	—	—	—	72.44 ± 11.3	1
12	024742.4+694904	02:47:42.48	69:49: 4.17	-0.01	0.67	<0.01	0.50	2.99 ± 1.6	1
13	032513.9+484555	03:25:13.96	48:45:55.46	0.19	0.88	<0.01	0.00	3.03 ± 1.3	1*
14	032655.9+485854	03:26:55.91	48:58:54.79	0.33	0.33	0.30	1.48	7.58 ± 1.1	1*
15	035956.3+541855	03:59:56.34	54:18:55.71	0.90	0.42	1.30	2.10	33.17 ± 4.7	1 [†]
16	041911.8+555243	04:19:11.87	55:52:43.24	0.32	-0.57	0.75	4.30	3.07 ± 1.4	3 [†]
17	045518.2+522938	04:55:18.27	52:29:38.76	0.76	0.31	0.80	1.90	1.80 ± 0.6	1
18	045555.7+304042	04:55:55.75	30:40:42.91	0.88	0.58	1.00	1.40	15.29 ± 1.1	1*
19	045825.2+515631	04:58:25.23	51:56:31.60	0.72	-0.00	0.85	2.80	23.17 ± 4.5	1 [†]
20	051541.7+471504	05:15:41.72	47:15: 4.83	0.04	0.72	<0.01	0.35	2.10 ± 1.0	1
21	051545.9+341346	05:15:45.91	34:13:46.58	0.78	0.27	0.90	2.35	295.38 ± 4.0	3 [†]
22	051556.9+460534	05:15:56.92	46:05:34.61	0.72	-0.09	0.98	3.10	1.86 ± 1.2	1
23	051646.0+340610	05:16:46.02	34:06:10.00	0.92	0.02	1.70	3.60	3.02 ± 1.1	1
24	051646.3+341410	05:16:46.36	34:14:10.43	0.58	0.49	0.44	1.26	18.33 ± 1.1	3 [†]
25	051745.2+455833	05:17:45.17	45:58:32.44	0.57	0.54	0.40	1.10	6.38 ± 2.0	1*
26	053845.2+282839	05:38:45.24	28:28:39.03	0.33	0.54	0.22	0.90	20.80 ± 6.5	1
27	063338.9+175933	06:33:38.88	17:59:32.15	—	—	—	—	8.18 ± 2.1	4
28	063528.3+052608	06:35:28.40	05:26: 8.69	-0.40	0.87	—	—	13.36 ± 4.4	1
29	063718.9+060832	06:37:18.90	06:08:32.62	0.25	0.96	—	—	61.02 ± 2.6	3 [†]
30	064038.3+094716	06:40:38.39	09:47:16.22	-0.19	-0.63	0.44	4.10	8.90 ± 0.4	2 [†]
31	064052.6+092952	06:40:52.61	09:29:52.29	-0.61	1.00	—	—	3.00 ± 0.5	6
32	064052.8+094857	06:40:52.86	09:48:57.80	0.50	0.69	0.25	0.60	2.45 ± 0.5	3 [†]
33	070435.4-114854	07:04:35.43	-11:48:54.24	—	—	—	—	20.75 ± 15.8	3 ^{††}
34	073651.2-303746	07:36:51.30	-30:37:46.69	0.52	0.02	0.60	2.40	33.41 ± 5.6	5 ^{††}
35	074646.2-192104	07:46:46.28	-19:21: 4.30	-0.04	0.00	0.21	2.10	11.10 ± 8.1	1 [†]
36	074731.3-191742	07:47:31.35	-19:17:42.40	0.64	-0.02	0.80	2.70	6775.41 ± 25.2	11 ^{††}
37	080332.6-400008	08:03:32.69	-40:00: 8.73	-0.40	-0.81	—	—	64.15 ± 4.2	2
38	080813.8-361432	08:08:13.88	-36:14:32.62	0.61	0.37	0.52	1.60	11.74 ± 4.3	1

Sources are presented in order of RA. The X-ray flux is in $\text{ergs s}^{-1}\text{cm}^{-2}$. It was computed in the SXSSC using an energy conversion factor (ECF) in the 0.2-12 keV energy band (details in XMM CAL-TN-0023-v2.0.ps report). N_H is in units of cm^{-2} . Flad-Id column refers to: 1- unidentified; 2- stars; 3- galaxie; 4- QSOs; 5- pulsar; 6- star forming region; 7- HII regions; 8- giant molecular clouds; 9- Herbig-Haro objects; 10- globular clusters and 11- cluster of galaxies. (★) - Source with radio detection at wavelength other than 20 cm. (†) - Source with 2MASS counterpart (Cutri et al. 2003).

1

1

Table 1: X-ray properties of NVSS/XMM-Newton cross-correlated sources

Src #	IAU name 2XMMp J+	Coordinates J2000		Hardness ratio		X-ray properties			flag Id.
		RA	DEC	HR _x	HR _y	N _H [10 ²²]	Γ	Flux[10 ⁻¹⁴]	
39	081446.6-185731	08:14:46.64	-18:57:31.84	0.68	-0.12	0.94	3.10	9.61 ± 2.7	1
40	083517.9-262458	08:35:17.98	-26:24:58.48	0.21	0.14	0.30	1.85	0.96 ± 0.4	1
41	083556.7-262610	08:35:56.75	-26:26:10.66	-0.46	0.49	<0.01	1.00	0.86 ± 0.6	1
42	083607.3-263754	08:36: 7.34	-26:37:54.71	—	—	—	—	10.08 ± 4.6	1
43	160833.8-390009	16:08:33.82	-39:00: 9.59	1.00	0.06	2.50	4.00	3.46 ± 0.8	2
44	165402.0-394630	16:54: 2.05	-39:46:30.36	0.61	0.85	0.22	0.00	8.52 ± 1.1	1 [†]
45	170102.8-295721	17:01: 2.87	-29:57:21.27	-0.27	0.74	—	—	4.37 ± 1.9	1 [†]
46	170806.1-322452	17:08: 6.19	-32:24:52.92	0.81	0.23	0.95	2.30	6.26 ± 2.9	1 [†]
47	170920.0-322439	17:09:20.07	-32:24:39.24	0.55	-0.09	0.70	2.80	7.02 ± 1.8	1
48	172231.6-234524	17:22:31.66	-23:45:24.34	0.26	0.53	0.18	0.90	0.48 ± 0.2	1
49	174405.9-293640	17:44: 5.96	-29:36:40.18	-0.14	0.87	—	—	5.14 ± 1.1	1 [†]
50	174720.2-282249	17:47:20.28	-28:22:49.38	-1.00	1.00	—	—	143.51 ± 20.2	8 ^{††}
51	174852.8-202136	17:48:52.81	-20:21:36.61	0.56	-0.24	0.80	3.25	58.13 ± 11.2	10 [†]
52	175017.4-312044	17:50:17.43	-31:20:44.14	-0.04	0.65	<0.01	0.50	4.50 ± 1.4	1
53	175446.8-300212	17:54:46.81	-30:02:12.26	0.63	0.23	0.62	1.90	2.30 ± 1.9	1
54	180306.8-222723	18:03: 6.89	-22:27:23.21	1.00	0.99	—	—	10.60 ± 3.1	1 [*]
55	180658.2-192724	18:06:58.21	-19:27:24.75	—	—	—	—	5.86 ± 2.5	1 ^{††}
56	180726.3-370038	18:07:26.36	-37:00:38.71	0.83	-0.38	—	—	0.84 ± 1.8	1
57	180754.3-202251	18:07:54.37	-20:22:51.84	0.92	0.15	1.30	3.10	2.37 ± 1.3	1 ^{††}
58	181006.4-194619	18:10: 6.48	-19:46:19.10	—	—	—	—	2.18 ± 0.6	1
59	181028.5-195547	18:10:28.59	-19:55:47.54	0.03	0.80	<0.01	0.10	19.37 ± 4.4	7 [†]
60	181856.1-205236	18:18:56.18	-20:52:36.35	0.43	0.35	0.36	1.50	1.11 ± 0.4	9 [†]
61	181904.0-210118	18:19: 4.02	-21:01:18.52	-1.00	1.00	—	—	0.93 ± 0.5	1
62	182702.5-110225	18:27: 2.56	-11:02:25.69	0.76	0.42	0.68	1.70	4.39 ± 1.9	1 [†]
63	183004.5+012234	18:30: 4.41	01:22:34.40	0.90	0.62	1.40	1.40	6.60 ± 0.9	6
64	183134.7-033538	18:31:34.75	-03:35:38.67	0.21	0.69	0.05	0.50	2.52 ± 0.9	1 ^{††}
65	183333.6-103406	18:33:33.56	-10:34: 6.33	0.93	0.60	1.40	1.70	7562.97 ± 15.1	5
66	184858.7-004810	18:48:58.78	-00:48:10.35	1.00	0.83	4.00	3.50	27.86 ± 8.6	1 [†]
67	184948.6-003708	18:49:48.63	-00:37: 8.98	-0.86	0.45	0.65	4.20	1.13 ± 0.9	1 ^{††}
68	191353.3+245603	19:13:53.37	24:56: 3.54	1.00	0.56	0.25	1.65	2.89 ± 1.0	1
69	193129.9+110208	19:31:29.96	11:02: 8.97	0.53	-0.30	0.80	3.40	2.45 ± 1.6	1
70	195309.7+325140	19:53: 9.73	32:51:40.15	0.18	-0.60	0.65	4.20	2.04 ± 1.6	1
71	201930.9+385018	20:19:30.97	38:50:19.00	0.20	0.23	0.25	1.65	0.57 ± 0.4	1 [†]
72	202017.1+402614	20:20:16.92	40:26:11.44	—	—	—	—	7.65 ± 2.0	1 ^{††}
73	202036.6+405753	20:20:36.57	40:57:52.03	—	—	—	—	47.99 ± 6.3	1 [*]
74	204258.2+274351	20:42:58.24	27:43:51.71	0.87	0.03	1.40	3.20	11.58 ± 3.2	3 [†]
75	204350.0+274045	20:43:50.05	27:40:45.08	0.47	-0.09	0.60	2.65	5.15 ± 1.3	1 [*]
76	210643.0+474152	21:06:43.00	47:41:52.98	-0.09	0.61	<0.01	0.65	7.12 ± 1.8	3 [†]
77	210653.0+385107	21:06:53.01	38:51: 7.23	0.24	-0.05	0.39	2.30	1.00 ± 0.7	1
78	211056.6+481620	21:10:56.70	48:16:20.07	0.85	0.06	1.30	3.10	11.81 ± 3.1	1 [*]
79	212634.1+375200	21:26:34.17	37:52: 0.58	1.00	-0.08	—	—	0.97 ± 0.7	1
80	214333.7+433259	21:43:33.77	43:32:59.97	0.65	-0.54	—	—	1.75 ± 1.2	3 [†]
81	220844.7+455553	22:08:44.75	45:55:53.02	0.86	0.26	1.30	2.40	3.18 ± 2.8	1
82	225346.6+605038	22:53:46.65	60:50:38.36	1.00	0.16	—	—	0.76 ± 0.4	1
83	225413.6+604513	22:54:13.62	60:45:13.68	0.46	0.62	2.60	0.80	0.71 ± 0.3	1
84	225444.0+604402	22:54:44.09	60:44: 2.21	1.00	0.69	—	—	1.62 ± 0.5	1
85	225554.8+604714	22:55:54.81	60:47:14.55	0.22	0.55	0.15	0.85	1.67 ± 0.7	1
86	233828.4+615832	23:38:28.47	61:58:32.14	0.67	0.24	0.68	2.00	34.89 ± 9.2	1